Somatosensory BOLD fMRI Reveals Close Link Between Salient Blood Pressure Changes and the Murine Neuromatrix

Reimann H.M., Todiras M., Hodge R., Huelnhagen T., Millward J.M., Turner R., Seeliger E., Bader M., Pohlmann A., Niendorf T.

This is the final version of the accepted manuscript. The original article has been published in final edited form in:

NeuroImage
2018 MAY 15 ; 172:562-574
2018 FEB 05 (first published online: final publication)
doi: 10.1016/j.neuroimage.2018.02.002

Publisher: Elsevier

Somatosensory BOLD fMRI Reveals Close Link Between Salient Blood Pressure Changes and the Murine Neuromatrix

Henning Matthias Reimann[1], Mihail Todiras[2], Russ Hodge[2], Till Huelnhagen[1], Jason Michael Millward[1], Robert Turner[3,4], Erdmann Seeliger[5], Michael Bader[2,6,7], Andreas Pohlmann[1], Thoralf Niendorf[1,6,8*]

[1] Berlin Ultrahigh Field Facility (B.U.F.F.), Max Delbrück Center for Molecular Medicine in the Helmholtz Association, Berlin, Germany

[2] Max Delbrück Center for Molecular Medicine in the Helmholtz Association, Berlin, Germany

[3] Max-Planck-Institute for Human Cognitive and Brain Sciences, Leipzig, Germany

[4] Faculty of Medicine, University of Amsterdam, Amsterdam, The Netherlands

[5] Institute of Vegetative Physiology, Charité – University Medicine, Berlin, Germany

[6] Department of Endocrinology, Charité – University Medicine, Berlin, Germany

[7] DZHK (German Centre for Cardiovascular Research), partner site Berlin, Germany

[8] Experimental and Clinical Research Center, a joint cooperation between the Charité Medical Faculty and the Max Delbrück Center for Molecular Medicine in the Helmholtz Association, Berlin, Germany

*** Corresponding Author:**

Thoralf Niendorf
Max Delbrück Center for Molecular Medicine in the Helmholtz Association
Robert-Rössle-Str. 10, 13125 Berlin, Germany
Tel: 0049 30 9406 4505, Fax: 0049 30 9406 4517
Email: thoralf.niendorf@mdc-berlin.de

Short title:

fMRI Reveals Link Between Blood Pressure and Neuromatrix

ABSTRACT

The *neuromatrix*, or "pain matrix", is a network of cortical brain areas which is activated by noxious as well as salient somatosensory stimulation. This has been studied in mice and humans using *blood oxygenation level-dependent* (BOLD) fMRI. Here we demonstrate that BOLD effects observed in the murine *neuromatrix* in response to salient somatosensory stimuli are prone to reflect *mean arterial blood pressure* (MABP) changes, rather than neural activity. We show that a standard electrostimulus typically used in murine somatosensory fMRI can induce substantial elevations in MABP. Equivalent drug-induced MABP changes — without somatosensory stimulation — evoked BOLD patterns in the *neuromatrix* strikingly similar to those evoked by electrostimulation. This constitutes a serious caveat for murine fMRI. The regional specificity of these BOLD patterns can be attributed to the co-localization of the *neuromatrix* with large draining veins. Based on these findings we propose a cardiovascular support mechanism whereby abrupt elevations in MABP provide additional energy supply to the *neuromatrix* and other essential brain areas in fight-or-flight situations.

Key words: mouse | BOLD fMRI | mean arterial blood pressure | pain matrix | pial veins | somatosensation | electrical stimulation

RESEARCH HIGHLIGHTS

- Standard electrostimulation evokes substantial MABP changes in mouse fMRI
- Equivalent drug-induced MABP changes (without electrostimuli) elicit significant BOLD patterns
- BOLD patterns preferentially occurred in brain areas of the “pain matrix”
- This can be explained by co-localization of the “pain matrix” with large pial veins
- The notion that autoregulation effectively buffers abrupt MABP changes of 60-120 mmHg was not confirmed

ABBREVIATIONS

BOLD = blood oxygenation level-dependent

CBF = cerebral blood flow

MABP = mean arterial blood pressure

HRF = hemodynamic response function

EV = explanatory variable

AngII = angiotensin II

Phe = phenylephrine

S1 = primary somatosensory cortex

$S1_{paw}$ = paw region of S1

S2 = secondary somatosensory cortex

ACC = anterior cingulate cortex

IC = insular cortex

PC = parietal cortex

1. INTRODUCTION

Nociception — the response of the sensory nervous system to painful stimuli — has evolved as an essential process to signal potential threats. It evokes immediate reactions to avoid injury, or to withdraw and seek safe refuge. This is critical to the survival of the organism.

Acute noxious stimuli have consistently been found to activate a bilateral pattern of brain areas that form the *neuromatrix* (Melzack, 1989), including the anterior cingulate cortex, the insular cortex, and the primary and secondary somatosensory cortices (Duerden and Albanese, 2011; Morton et al., 2016; Tanasescu et al., 2016). This network, often referred to as the "pain matrix" (Iannetti and Mouraux, 2010), appears to alert the organism to the presence of danger, and triggers prompt and appropriate motor responses (Haggard et al., 2013; Legrain et al., 2011; Mancini et al., 2014). The importance of the *neuromatrix* for survival is underscored by its evolutionary conservation across species. Electrophysiological techniques applied to humans, rats and mice have confirmed a key role of the corresponding brain areas in nociception (Flaten and al'Absi, 2015), thus emphasizing how studies in animal models may be usefully extrapolated to the human context.

The "pain matrix" has primarily been studied using *functional magnetic resonance imaging* (fMRI), based on the *blood oxygenation level-dependent* (BOLD) effect (Morton et al., 2016). BOLD fMRI is effective for studying large-scale neural networks across the entire brain non-invasively by mapping local changes in blood oxygenation (Kim and Ogawa, 2012; Ogawa et al., 1990). During increased activity, neurons mediate vasodilation in adjacent capillaries and precapillary arterioles, which leads to an increase in local blood flow and enables enhanced energy supply to the activated cells (Hall et al., 2014; Hamilton, 2010). The resulting rise in local blood oxygenation can be detected due to the different magnetic properties of oxygenated and deoxygenated hemoglobin (Kim and Ogawa, 2012; Ogawa et al., 1990). This is the canonical model of neurovascular coupling in which the BOLD effect serves as a surrogate for neural activity.

However, there is growing evidence that BOLD effects observed in the murine *neuromatrix* in response to acute noxious and somatosensory stimuli may not be evoked exclusively by neural activity (Reimann et al., 2016; Schroeter et al., 2016; Schroeter et al., 2014). Acute noxious stimuli may induce abrupt increases in *mean arterial blood pressure* (MABP) (Jeffrey-Gauthier et al., 2013; Uchida et al., 2017). In rats it was shown that abrupt and strong elevations in MABP (by >40mmHg) can increase the influx of oxygenated blood into the brain vasculature, where it translates into wide-spread BOLD effects (Kalisch et al., 2001; Tuor et al., 2002; Tuor et al., 2007; Wang et al.,

2006). Such confounding effects would correlate with the applied stimulus, and might thus be indistinguishable from those evoked by neurovascular coupling. While studies in rats have suggested that cerebral autoregulation maintains *cerebral blood flow* (CBF) virtually constant against MABP changes within a range of 60-120 mmHg (Gozzi et al., 2007; Ferrari et al., 2012), it has not been studied yet whether dynamic autoregulation could buffer such abrupt MABP changes in mice. Additionally, the magnitude of MABP elevations evoked by standard somatosensory stimuli used in mouse fMRI is entirely unknown.

It was previously shown that mild noxious heat stimuli applied to the murine paw caused abrupt and transient increases in MABP of about 20 mmHg (Reimann et al., 2016). Although the resulting BOLD patterns appeared to be focused in the "pain matrix" and other brain areas known to be involved in nociceptive processing, it became clear – when a less stringent statistical standard was applied – that the significant patterns were peak regions of an underlying global BOLD effect (Reimann et al., 2016). Similar global BOLD effects have been described in response to standard somatosensory electrostimulation of the murine paw, also with peak regions in key areas of the "pain matrix" and in thalamic nuclei (Schroeter et al., 2014).

These observations raised the question of whether those BOLD patterns originate from underlying neural activity or if they are confounded or even entirely evoked by changes in MABP (Schroeter et al., 2016; Reimann et al., 2016), which could have profound implications for research into somatosensory fMRI in mice. If the observed BOLD patterns were indeed evoked only by MABP changes, it remains unclear why they occur reliably in brain areas of the *neuromatrix*.

To pursue these questions we conducted functional MRI in mice, i) to elucidate the relation of BOLD response and associated MABP changes induced by standard electrical stimulation; and ii) to investigate BOLD effects induced by pharmacologically evoked MABP changes with no somatosensory stimulation. Our findings demonstrate that the interpretation of BOLD signals in mouse fMRI can be severely confounded by MABP alterations, even within the presumed range of virtually perfect autoregulation. A novel explanatory model is proposed that explicitly includes a close link between salient blood pressure elevations and the murine neuromatrix.

2. METHODS

2.1 Animal experiments

Animal experiments were carried out in accordance with the guidelines provided and approved by the Animal Welfare Department of the *Landesamt für Gesundheit und Soziales* (LaGeSo) Berlin (Berlin State Office of Health and Social Affairs). All mice were housed in groups of 4-6 animals in cages with nesting material, mouse lodges and open access to water and feed, at 24 °C with a 12 h/12 h circadian cycle.

2.1.1 Animal preparation. Male C57BL/6N mice (weight 23-28 g) were anesthetized using isoflurane (induction: 2-3% isoflurane, maintenance: 1.2-1.5% isoflurane, in an 80%/20% air/ oxygen mixture), endotracheally intubated and mechanically ventilated to ensure stable physiology (90 bpm). The left femoral artery was cannulated to allow for continuous monitoring of mean arterial blood pressure (MABP). MABP was stable throughout the experiment. The mice were positioned in a customized mouse bed, which encloses the whole body and ensures overall homogenous body temperatures of 36.3±0.5°C (Reimann et al., 2016). The head was stereotactically fixed using a tooth bar and customized earmuffs (together with moldable ear wax) to avoid distraction by acoustic noise of the gradient system. Catheter was connected to the measuring column, a pair of needle electrodes was subcutaneously injected into the right hind paw, and the mouse bed was immediately transferred into the magnet. For fMRI acquisitions anesthesia was reduced to 1.0% isoflurane. Each fMRI session consisted of 3 subsequent functional scans of different tasks including electrostimulation and the administration of vasoconstrictive drugs (see stimulation paradigms). The first functional scan was started approximately 60 min after induction and 15 min after reduction of isoflurane. To prevent motion the animals were immobilized prior to fMRI using a muscular blocking agent (pancuronium bromide, 1mg/kg). MABP was monitored throughout the experiment (PowerLab, ADinstruments). From those recordings heart rate signal time courses were extracted. Each fMRI time series was introduced by a trigger signal to synchronize the MABP recording with the data acquisition.

2.1.2 Stimulation paradigms. Functional scans were acquired in the following order: First, electrical stimulation of the paw (scan time: 10 min), second, administration of phenylephrine, and third, of angiotensin II (scan time each: 5 min). Electrostimulation paradigm was conducted in 4 subsequent pulse trains (1mA, 0.5ms, 12Hz) of 15 seconds with each onset starting after 120 seconds. Drug administration (i.v.) was conducted 120 seconds after the scan started using either

phenylephrine (10µg/kg) or angiotensin II (500ng/kg). Scans were interleaved by a resting period of 10 min (electro /phenylephrine) and 20 min (phenylephrine /angiotensin II), respectively.

2.1.3 Magnetic resonance imaging (MRI). MRI experiments were performed on a 9.4 Tesla Bruker small bore animal MR system (BioSpec 94/20, Bruker BioSpin, Ettlingen, Germany). A cryogenic quadrature radiofrequency (RF) probe (CryoProbe, Bruker BioSpin, Ettlingen, Germany) was used for signal transmission and reception (Niendorf et al., 2015). The CryoProbe thermal shield was adjusted to physiological preserve scalp temperatures of 36.0 °C ± 0.5 °C (Reimann et al., 2016).
Pilot images and high spatial resolution saggital T_2-weighted images were used to position the structural reference scan, which consisted of 19 axial T_2-weighted slices (RARE, echo train length 16, TR 3344 ms, TE 49.3 ms, FOV (16x12x11.4) mm^3, matrix 160x120, resolution (100x100) μm^2, slice thickness 500 µm, slice spacing 600 µm) covering the entire mouse brain. Prior to fMRI magnetic field homogeneity was improved by voxel-based shimming using the MAPSHIM technique, which calculates the 1st and 2nd order shims for a defined volume of interest (shim voxel) based on an acquired B_0 field map. The geometry of the shim voxel was set such that it covers the dorsal part of the brain excluding the air filled anterior cavities. For T_2^*-weighted fMRI stacks of 19 axial slices were acquired using gradient echo echoplanar imaging (GE-EPI, TR 2500 ms, TE 11.0 ms, flip angle 80°, FOV (16x12x11.4) mm^3, matrix 80x60, resolution (200x200) μm^2, slice thickness 500 µm, slice spacing 600 µm, bandwidth 300 kHz) and a temporal resolution of 2.5 s. Susceptibility-weighted structural MRI data were acquired using gradient echo echoplanar imaging (GE-EPI, TR 5000 ms, TE 11.0 ms, flip angle 80°, FOV (16x12x11.4) mm^3, matrix 160x120, resolution (100x100) μm^2, number of slices 19, slice thickness 500 µm, slice spacing 600 µm, bandwidth 300 kHz). To allow for post-acquisition distortion correction of the functional scans another 3D B_0-map was acquired with the same geometry used for the functional scans, but in 3D mode using a matrix size of 80x60x19 and a FOV of (16x12x11.4) mm^2.

2.2 Data processing and analysis.

MRI data were processed by an in-house built processing pipeline (written in UNIX shell scripts). All analyzing and processing tools employed are part of the FMRIB's Software Library (FSL, Oxford, UK) (Jenkinson et al., 2012) if not stated otherwise. Prior to image processing MR data were converted to NIFTI-format and scaled to human dimensions (x,y,z-voxel size x20) to better meet the requirements of human fMRI data processing and display.

2.2.1 fMRI data processing. Functional time-series were motion corrected (MCFLIRT) and EPI distortion correction was applied via FUGUE to account for magnetic field inhomogeneity induced image distortions. Structural image volumes were filtered using a *spatially adaptive non-local means* (SANLM) filter (Manjon et al., 2010) and skull stripping was performed using the *brain extraction tool* (BET). Spatial normalization to an anatomical reference (Janke et al., 2012) was applied using non-linear diffeomorphic image registration by explicit B-spline regularization (Tustison and Avants, 2013), which is part of the Advanced Normalization Tools "ANTs" (Avants et al., 2011).

2.2.2 Statistical analysis. Smoothing was applied with a FWHM of 6 mm (which accords to 300 µm) (SUSAN) and fMRI data processing was carried out using FEAT (FMRI Expert Analysis Tool) Version 6.00, part of FSL. Data from the initial 4 time points of a time-series were discarded to exclude hardware and saturation related artifacts. 4D data was high pass filtered with a cut-off of 135 seconds equaling one stimulus duration plus the initial baseline period. General linear model analysis was performed by convolving a binary (0 = off, 1 = on) *explanatory variable* (EV) with a double-gamma function (FSL /SPM preset: a standard positive gamma function (σ = 2.449 s) at normal lag (delay = 6 s), mixed with a small (ratio = 1/6), delayed (16 s), inverted gamma (σ = 4 s), which attempts to model the late undershoot) and its temporal derivative (Glover, 1999; Friston et al., 1998). The same temporal filtering was applied to the HRF model as to the data, to obtain the best possible match between the model and data. The duration of the EV was set to 15 seconds in all conditions regardless the actual length of MABP response to test a possible confounding effect of systemic blood pressure increases to the common *general linear model* analysis using an *hemodynamic response function* (HRF) model as EV. By applying the MABP as EV to the *general linear model* analysis the actual transition slope and duration of the MABP curve were taken into account.

2.2.3 Second level analysis. Higher-level modeling was conducted using full FMRIB's local analysis of mixed-effects (FLAME, stages 1+2). Group z-statistic maps were thresholded using cluster-based inference determined by z = 2.3 (which equals a primary or cluster-defining threshold of $p<0.01$) and a cluster-level extent threshold of $p<0.05$ that controls family-wise error rate. Resulting z-maps were further compared using a more stringent primary threshold of $p<0.001$ (Woo et al., 2014; Eklund et al., 2016). For conjunction group analysis single subject z-statistic maps were thresholded at z = 2.3 ($p<0.01$), binarized (0 = not significant, 1 = significant), added up for the

respective groups, and displayed in percentage. Resulting maps were thresholded at 30% to match the defined criterion. All maps were superimposed on a high-resolution anatomical 3D image volume, which was normalized to the anatomical reference (Janke AL, 2012).

2.2.4 Anatomical classification. Spatial overlaps of significant clusters with anatomical brain regions were identified by applying anatomical atlas masks (Ullmann et al., 2013; Watson et al., 2017) onto the group z-statistic map. Atlas masks are available from the webpage of the Australian Mouse Brain Mapping Consortium (http://www.imaging.org.au/AMBMC) in the same coordinate space as the reference model (Janke et al., 2012) applied for spatial normalization.

2.2.5 BOLD signal time courses. Signal time courses were created for significant voxel clusters in specified anatomical regions. Atlas masks for specified anatomical brain regions were applied to the functional time series and used to extract intensity time courses for each subject. Best voxel time courses were extracted from voxels with the highest z-scores. Signal change (%) was calculated ((signal * 100 / baseline) - 100) and averaged over all animals.

3. RESULTS

3.1 BOLD and MABP changes induced by standard electrical stimulation

We first tested the hypothesis that a standard subcutaneous electrostimulation of the murine hindpaw (1mA, Fig. 1) elicits an observable increase in MABP. The first stimulation period provoked an increase in MABP of 20.2±3.8 mmHg, which rose with a transition rate (tr) of 2.9 mmHg/s from a stable baseline of 88.3±2.7mmHg (mean ± s.e.m.). The second pulse train led to a markedly lower magnitude of MABP increase (11.3±3.1 mmHg) with a slower transition (tr = 1.8 mmHg/s), and a further decline was observed for subsequent blocks of pulse trains. These findings demonstrate that a 1mA electrostimulation can cause substantial increases in MABP in mice, although well within the presumed range of perfect dynamic autoregulation (60-120 mmHg).

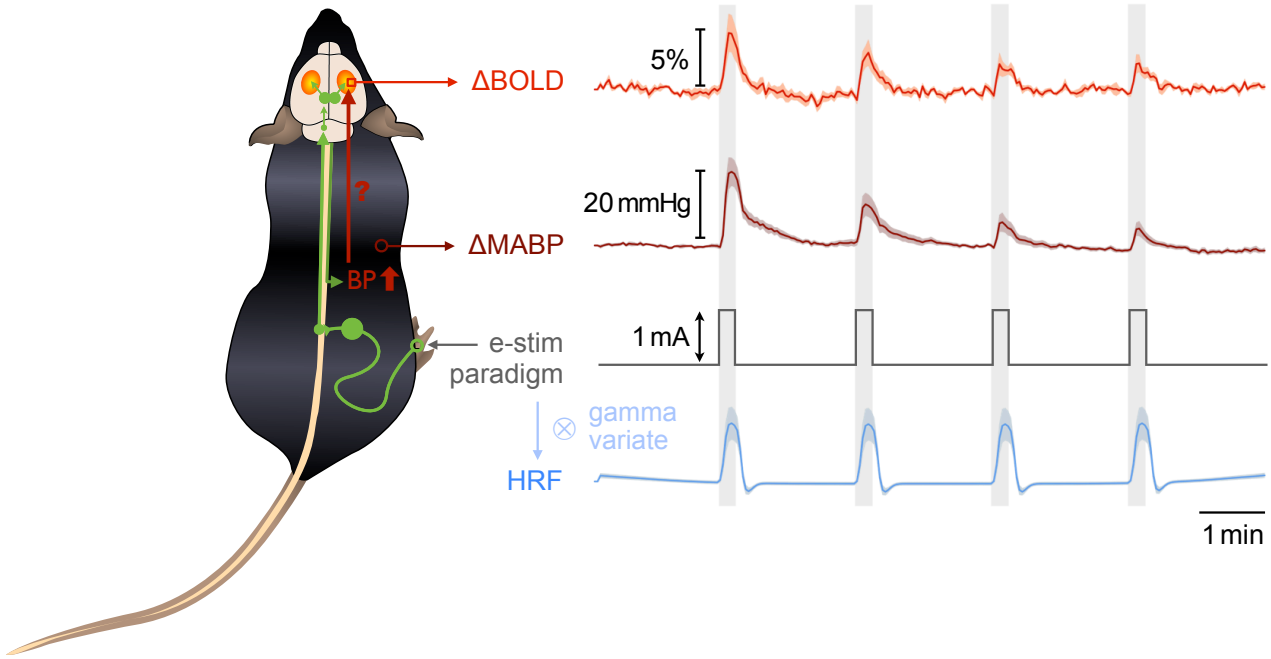

Fig.1 – Left panel: Current model in somatosensory mouse fMRI. Application of electrical stimuli to the hindpaw entails signal transmission into brain areas of the neuromatrix. Neurovascular coupling causes local changes in blood oxygenation in activated areas. Stimulus evoked alterations in MABP could contribute to the occurrence of BOLD effects in the neuromatrix. **Right panel: Signal time courses. ΔBOLD.** Signal intensity time courses in response to electrical stimulation of 1mA plotted for those voxels, which exhibit the highest correlation with the HRF model (for details see Fig. 3a). **ΔMABP.** Changes in MABP in response to the same stimulus. **HRF.** Hemodynamic response function generated by convolution of the electrostimulation paradigm with gamma functions. All curves plotted as group mean of 7 mice (± s.e.m.).

When this paradigm was applied as a standard somatosensory fMRI task, significant voxel clusters were detected bilaterally in large sections of the primary somatosensory cortex (S1) (Fig. 2). These regions included the barrel field and in particular the S1 region, which processes somatosensory input from the paw ($S1_{paw}$). Bilateral significant clusters were also observed in the secondary somatosensory cortex (S2), anterior cingulate cortex (ACC), ventral nuclei of the thalamus including ventrolateral (VL) and ventral posterolateral thalamic nuclei (VPL), and the posterior thalamic nuclear group (Po). These BOLD patterns concur with prior reports of murine fMRI (Baltes et al., 2011; Bosshard et al., 2010; Petrinovic et al., 2016; Schroeter et al., 2014). Respective brain regions of the contra- and ipsilateral hemispheres showed clear correspondences in their BOLD signal changes over time (Fig. 2c, right panel). All BOLD signal traces plotted for the selected regions exhibited a decline in signal magnitude for subsequent pulse trains.

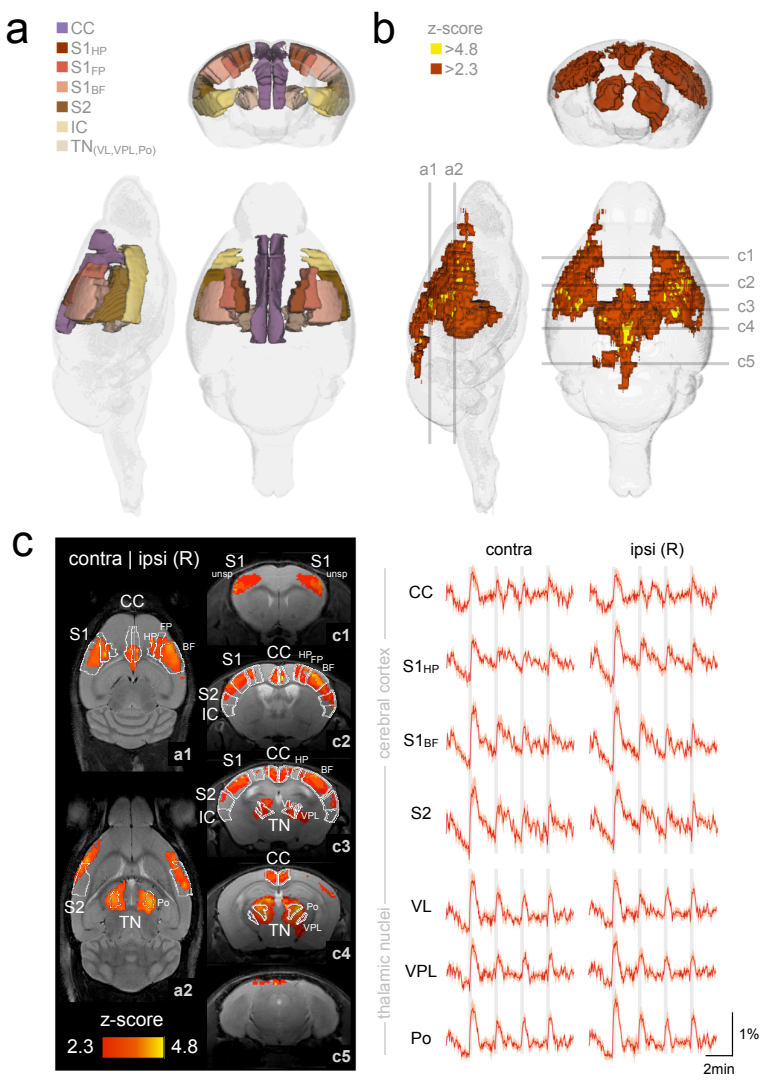

Fig. 2 – BOLD effects in the mouse brain in response to electrostimulation.

a. Anatomical areas of the neuromatrix (also known as „pain matrix"), which match cortical and thalamic significance patterns in response to electrostimulation in the mouse brain (b,c): cingulate cortex (CC), insular cortex (IC), primary somatosensory cortex (S1) including somatotopic representation areas for the hindpaw (HP), forepaw (FP), and barrel field (BF), the secondary somatosensory cortex (S2), and thalamic nuclei (TN) including ventrolateral (VL), ventral posterolateral (VPL), and posterior thalamic nuclei (Po). **b.** Spatial BOLD distribution in response to electrostimulation in mice reveals symmetric and bilateral patterns (n=9, mixed effects analysis, cluster based inference, p<.05). **c. Left panel:** 2 axial and 5 coronal slices taken from the labeled positions in b. Z-scores are color coded. Anatomical areas are outlined in white. **Right panel:** Group average BOLD signal time courses (± s.e.m.) for significant voxels in anatomically defined areas in the contra- and ipsilateral hemisphere in response to electrostimulation (grey shadings). Note the great correlations in time courses of similar regions in ipsi- and contralateral hemisphere.

To obtain these results we performed a linear regression based on a *general linear model*, which is the most common way to analyze task-related fMRI data (Poline and Brett, 2012). Here the stimulation paradigm is convolved with a gamma variate curve to form a *hemodynamic response function* (HRF, Fig. 1, bottom). The HRF is the canonical prediction of the BOLD response to local changes in neural activity with respect to the stimulation block paradigm, and it is used as an *explanatory variable* (EV) by correlating it with the signal time course of every voxel in the mouse brain (Fig. 3a). The resulting statistical z-map displays the z-scores of all tested voxels based on their correlation with the input EV, after application of a default statistical threshold to avoid false positive errors (Eklund et al., 2016).

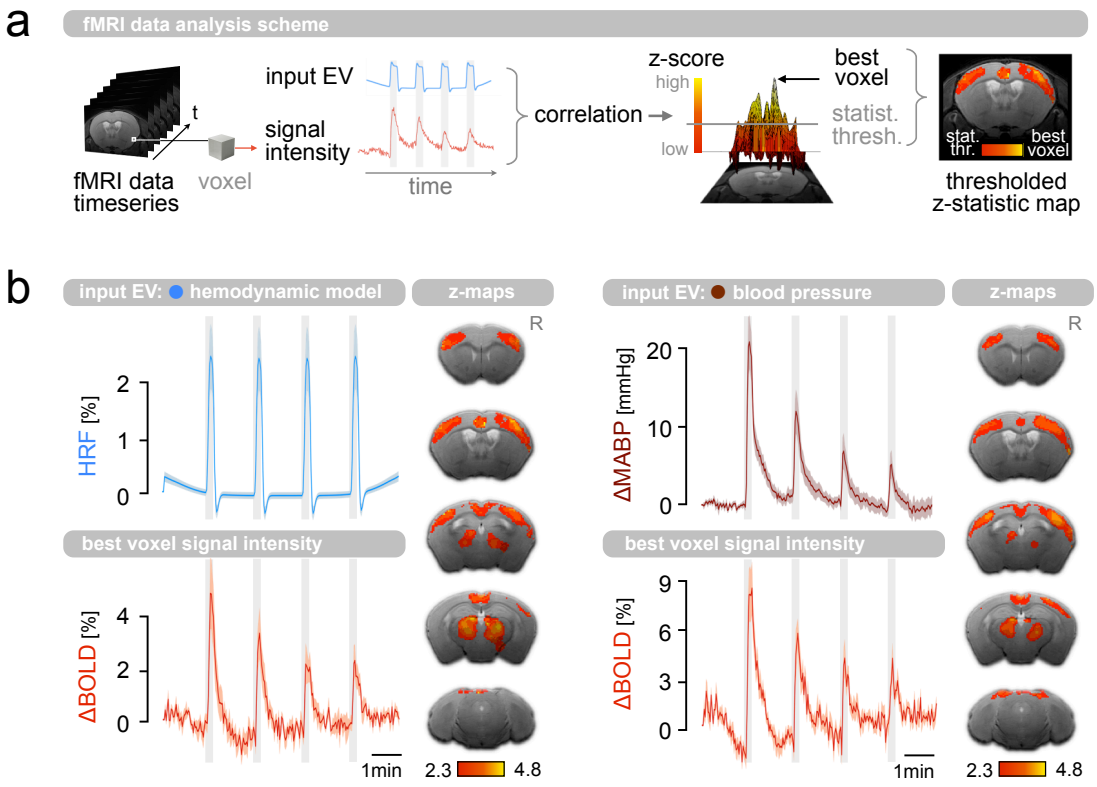

Fig. 3 – a. Data analysis scheme. A general linear model was used to test the extent by which the signal intensity time course of each voxel in the mouse brain can be described by a defined input EV. The higher the correlation between both curves, the higher is the z-score of a tested voxel. The voxel with the highest z-score is defined as „best voxel“. A statistic threshold was introduced based on default statistic inference to exclude false positive errors. **b. Comparison of statistical group analysis for electrostimulation using either HRF or MABP as EV.** Mixed effects analysis (n=9), cluster based inference (p<.05), 5 representative brain slices. Z-statistic maps and BOLD plots for the same mice during electrostimulation of the hindpaw. **Left panel:** Subjects were analyzed using an HRF as EV based on the stimulus. **Right panel:** Signal time course of the MABP was used as EV, which was monitored during the fMRI session. Group average BOLD signal curves are plotted in red (mean ± s.e.m.) with stimulation periods shaded grey. Right side labeled with R. Spatial distribution of best voxels are shown in figure 7.

Next we examined whether the MABP changes could influence, or possibly even cause the BOLD effects in the mouse brain. For this purpose we monitored MABP during each fMRI session and employed the MABP signal trace as an EV in the *general linear model* analysis for each subject. The group analysis revealed a spatial distribution of significant clusters in the statistical maps which was almost identical to the brain mapping pattern obtained when an HRF based on the electrostimulation paradigm was used (Fig. 3b). The MABP signal trace closely corresponded to the BOLD signal time courses in the brains of all animals. Compared to the BOLD signal of those brain voxels which best correlated with the MABP time course, the “best voxels” determined for the HRF analysis showed a slightly faster transition in returning to the baseline.

Taken together, we found i) that electrostimulation evoked stimulus-correlated alterations in MABP, and ii) that the BOLD signal in the mouse brain reflected the MABP time course. When the MABP trace was used as an EV, the z-statistic maps revealed the same BOLD voxel clusters as the HRF expected for electrostimulation.

3.2 BOLD effects evoked by pharmacologically induced MABP changes

The above findings demonstrate that the impact of MABP changes induced by electrical stimulation is intrinsically incorporated in the murine BOLD response. It remains to be elucidated to what extend the BOLD effect reflects elevated MABP rather than neural activity in response to the electrical stimulus, or some combination of both. The contribution of MABP on the BOLD signal can be investigated by inducing increases in MABP in the absence of any somatosensory stimulation, and examining the effects on the BOLD signal. To accomplish this we used two vasoconstrictive agents to mimic the blood pressure alterations evoked by electrostimulation: angiotensin II (AngII) and phenylephrine (Phe). The separate use of two different agents acting on different receptor types provides a safeguard to reveal the effects of MABP elevation on the BOLD signal: if similar BOLD patterns are observed in response to both agents, any possible effects not caused by MABP elevations can be considered negligible. For each vasoconstrictive agent the dose was set to achieve MABP increases comparable with those evoked by electrical stimulation (ΔAngII = +21.5±4.0 mmHg, ΔPhe = +20.4±2.9 mmHg) with transition rates of 3.1 mmHg/s for AngII and 3.2 mmHg/s for Phe (Fig. 4). Elevations in MABP were accompanied by distinct changes in heart rate with comparable transition rates, but with a delayed onset of several seconds, out of a stable baseline of 520.6±23.6 bpm for all conditions. An average increase in heart rate of +31.8±8.5 bpm was observed in response to electrostimulation, while the average heart rate decreased by -51.0±17.8 bpm and -71.6±11.7 bpm in response to AngII and Phe, respectively.

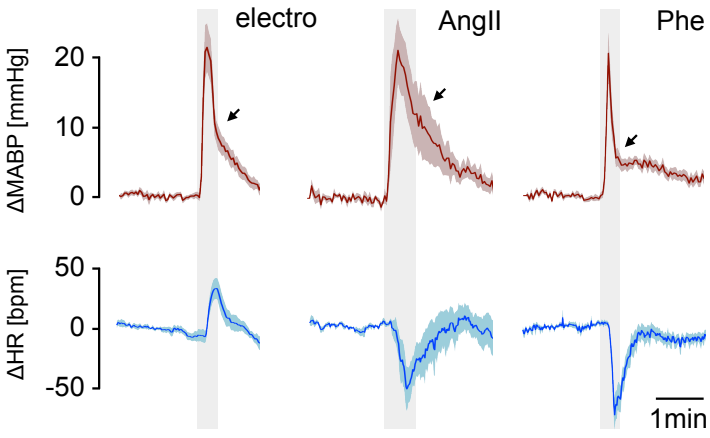

Fig. 4 – Changes in MABP and heart rate (HR) in response to electrostimulation and vaso-constrictive agents. Group average time courses (± s.e.m.) for ΔMABP and ΔHR monitored during electrostimulation (n=9), AngII (n=6) and Phe (n=15). Both agents were used to evoke MABP alterations comparable to those observed in response to electrostimulation. All ΔMABP curves show an initial, rapid phase of decay and a second, slower phase (separated by black arrow). ΔHR increases with ΔMABP for electrostimulation and decreases for vasoconstrictive agents. All curves were monitored during the actual fMRI experiment.

MABP was continuously monitored during AngII and Phe administration, and was used as an EV for the *general linear model* analysis at the single subject level. The time courses obtained by monitoring MABP were accurately reflected in the BOLD signals for both interventions, AngII and Phe (Fig. 5a). Mixed-effects group analyses revealed significant voxel clusters predominantly in the ACC, the ectorhinal cortex at the boundary of the posterior insular, and S1, particularly in the area encoding for sensory input of the right paw. Additional clusters were observed bilaterally in the parietal cortex.

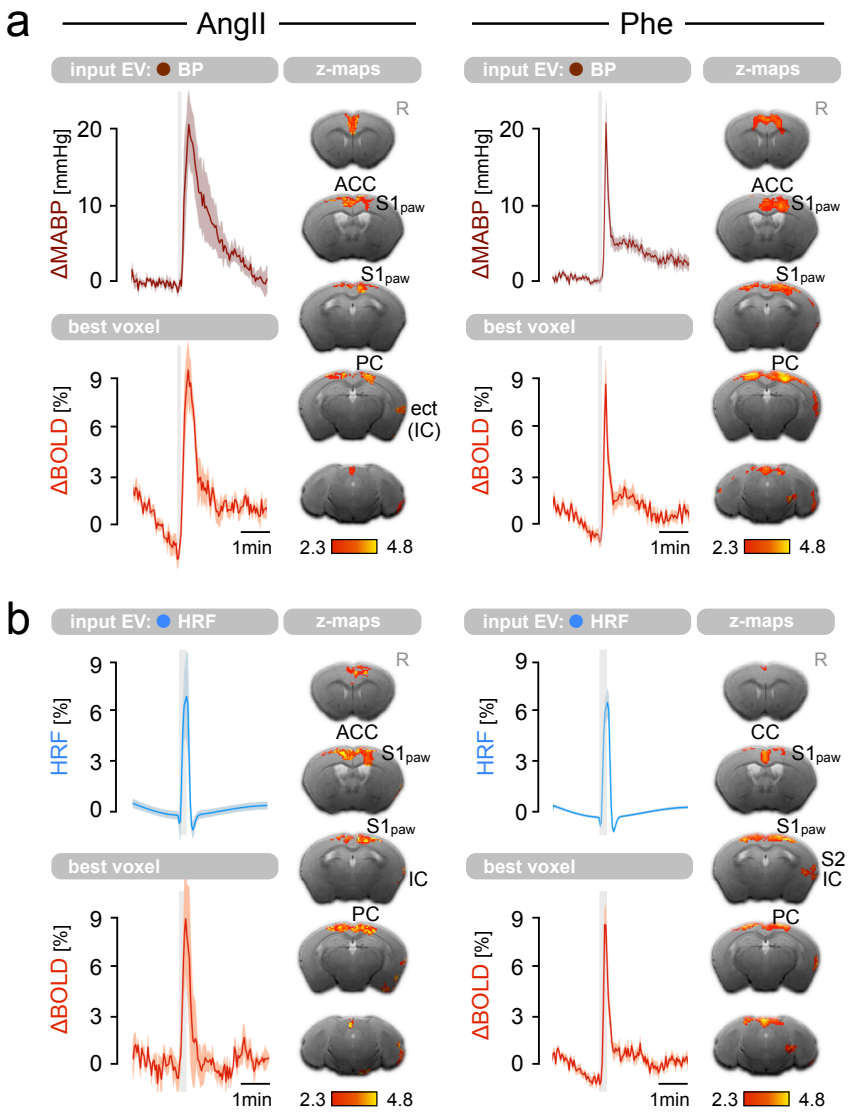

Fig. 5 – Comparison of statistical group analysis for vasoconstrictive agents. Mixed effects analysis, cluster based inference (p<.05), 5 representative brain slices. Statistic z-score maps and group average BOLD plots (± s.e.m.) for subjects treated with angiotensin II (AngII, n=6) or phenylephrine (Phe, n=15). **a.** Subjects were analyzed using ΔMABP as input EV, which was monitored during the fMRI session. Grey shades indicate pharmacological injection times (~5 sec). **b.** Subjects were analyzed using an HRF as regressor, which is based on the electrostimulation block paradigm (grey shadings). Significant voxels were found in anterior cingulate cortex (ACC), primary (S1) and secondary somatosensory cortex (S2), ectorhinal (ect) and insular cortex (IC), and the parietal cortex (PC). Right side labeled with R.

The pharmacologically induced MABP alterations were generated to be as similar as possible to those elicited by electrostimulation. Since the MABP time course was indeed reflected in the BOLD signal of the mouse brain we hypothesized that similar spatial BOLD patterns would be detectable for an HRF deduced from using the electrostimulation block paradigm as EV. The group analysis revealed a spatial distribution of significant voxel clusters which corresponded very well to the spatial pattern observed when using the MABP as EV, for both angiotensin II and phenylephrine interventions (Fig. 5b). BOLD clusters in the right posterior insular cortex became significant for Phe, extending into the anatomical area of S2. In contrast with the BOLD patterns observed for electrostimulation, no significant voxels were found in the thalamic nuclei, or in the barrel fields, irrespective of which EV was used.

The group-averaged BOLD signal time courses shown in figure 3 and 5 were calculated from those voxels which showed the best correlation with the respective EV (as defined by the correlation coefficient) for each task in each subject. Regardless of which EV was used, these “best voxels” were found exclusively in superficial cortical layers of the mouse brain (Fig. 6).

To summarize, i) we reproduced pharmacologically the MABP alterations observed in response to electrostimulation. ii) The pharmacologically induced MABP changes were sufficient to evoke significant BOLD clusters which survived a mixed-effects group analysis. iii) Similar BOLD patterns were observed regardless of whether the monitored MABP or an HRF based on the electrostimulation paradigm was used as the EV for the *general linear model* analysis. iv) Voxels which correlated best with the input EV (HRF and MABP) were located in superficial layers of the mouse brain. v) The spatial distribution of BOLD patterns overlapped with those evoked by electrostimulation, most notably the area for somatosensory representation of the paw, but vi) in the absence of somatosensory stimulation, no significant clusters were found in thalamic nuclei.

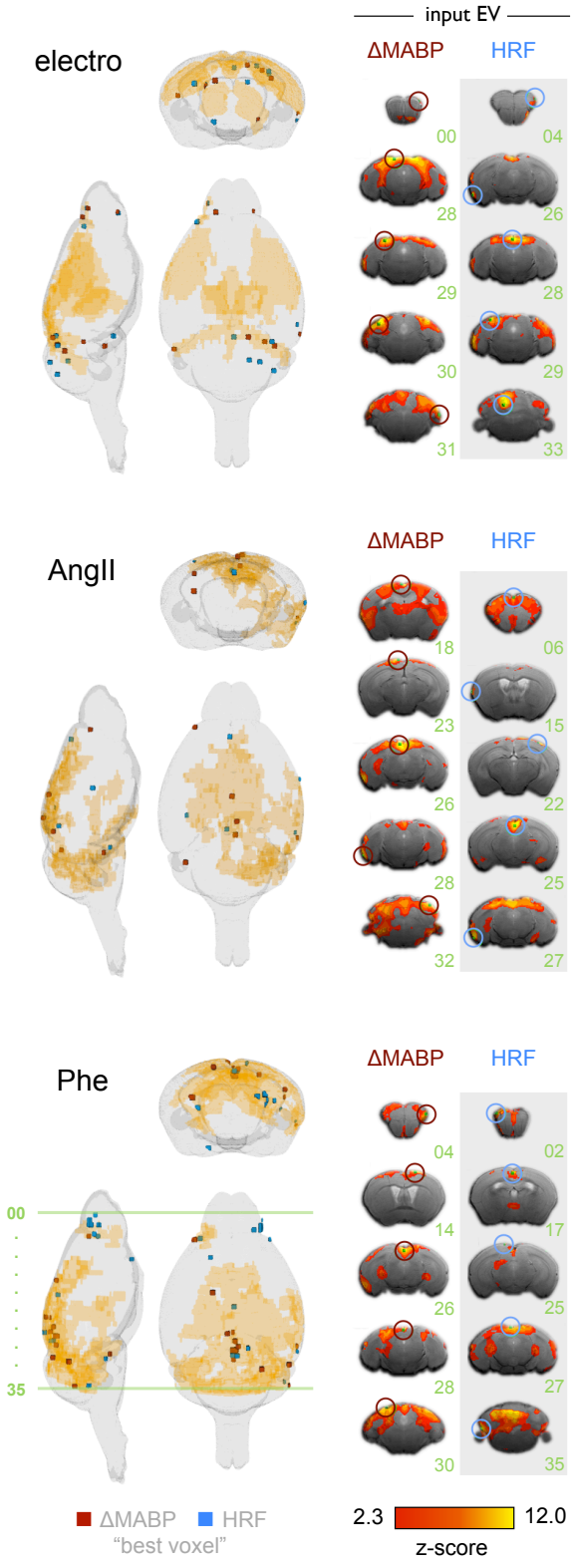

Fig. 6 – Best voxel location. Location of voxels, which correlate the best with the applied EV – either an HRF based on the electrostimulation paradigm or the time course of the MABP. **Left panel:** Distribution of best voxels (based on single subject analysis) projected on a glass brain displaying a merge of significant voxel patterns from group analyses for both EVs (ΔMABP and HRF). Best voxels for $EV_{\Delta MABP}$ are shown in red, best voxels for EV_{HRF} in blue. **Right panel:** Representative slices of individual subjects. Best voxels are circled in red ($EV_{\Delta MABP}$) or blue (EV_{HRF}) and slice numbers are shown in green.

3.3 Detailing the effects of MABP alteration in fMRI analyses

The previous experiments demonstrated that changes in MABP elicited significant spatial clusters in the mouse brain upon mixed-effects group analysis. To achieve a high sensitivity, we adopted the commonly used primary threshold of p<0.01. Nevertheless, the principle cluster patterns were still preserved, even when using a more stringent primary threshold of p<0.001 (recently suggested by Woo et al., 2014 and Eklund et al., 2016) (Fig. 7). The stringent thresholding generally resulted in smaller cluster sizes. The smaller clusters that were detected only at p<0.01 included BOLD patterns in the ACC and thalamus in response to electrostimulation, and small lateral patterns in the IC and S2 in mice treated with AngII and Phe (Fig. 7, indicated by arrows).

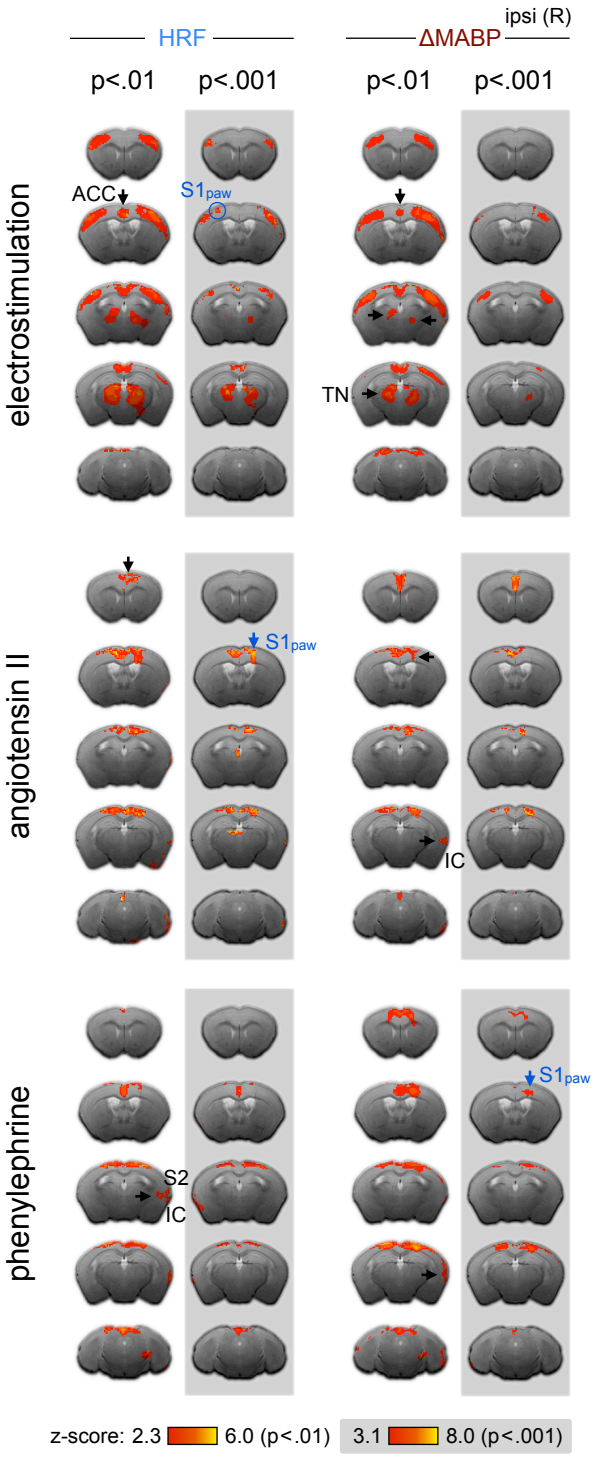

Fig. 7. Comparison of group z-statistic maps at liberal and stringent primary thresholds. To test the impact of MABP on the BOLD signal at more conservative inference, clusters at primary thresholds of p<0.01 were compared with p<0.001 for all conditions (electrostimulation, AngII and Phe, using HRF or MABP as an input EV. While the more stringent primary threshold of p<0.001 generally resulted in smaller cluster sizes, the principle cluster patterns were preserved with few exceptions. Electrostimulation: clusters in the ACC remained only visible at p<0.01. Thalamic clusters showed a better correlation with HRF than with MABP, which holds also true for the small cluster in the paw region of contralateral S1 (blue circle). Vasoconstrictive agents: clusters in the ipsilateral paw region survived thresholding at p<0.001 in AngII (HRF) and Phe (MABP) (blue arrows). Small lateral clusters in S2 and IC were detected only at p<0.01.

This type of analysis deems as significant only those voxel clusters which hold high z-scores in the majority of subjects. This is the prevailing strategy used in functional MRI to ensure group effects with high consistency across subjects (Woo et al., 2014; Eklund et al., 2016). However, this approach does not fully cover the entire scope of brain regions which might be affected by MABP changes. We therefore elaborated on spatial BOLD distribution at the level of single subjects, and followed this up by linking it to the neurovascular system.

i) Conjunction maps

Conjunction analysis straightforwardly summarizes the results of single subject maps by counting in how many animals a corresponding voxel was significantly activated. This requires rendering statistical maps of all the animals tested in each group, converting them into binary masks (1 = significant, 0 = not significant), adding up these masks and finally displaying the total count as a percentage of the number of animals. The method has the virtue of depicting the whole range of significant voxels that survived the statistical inference in a single subject analysis, thus permitting identification of overlaps between clusters in multiple subjects. Figure 8a (top panel) shows group conjunctions for mice treated either with electrostimulation or pharmacological interventions and analyzed using individual MABP traces as EVs, as described above.

The conjunction analysis revealed that BOLD patterns in single subjects were not restricted to specific brain regions. Instead, the BOLD clusters appeared widely distributed over large parts of the brain, forming a symmetrical bilateral pattern under all conditions (Fig. 8a, left panel). To identify the hot spots of more consistent BOLD aggregation across subjects we set a threshold to only display voxels that were significant in at least 30% of the animals (Fig. 8a, right panel). Using this approach a difference map was generated to compare BOLD clusters evoked by somatosensory stimulation with those evoked by pharmacological increase of systemic blood pressure (Fig. 8b, left column). Anatomical brain areas that were consistently determined as significant under both conditions include the fore- and hindpaw regions of the primary somatosensory cortex, the S2, ACC, IC, PC, and the boundary between the hippocampus and thalamus. Areas that reached significance only in response to electrostimulation but not to pharmacological blood pressure elevations include $S1_{BF}$, and the (ventral) thalamic nucleus groups.

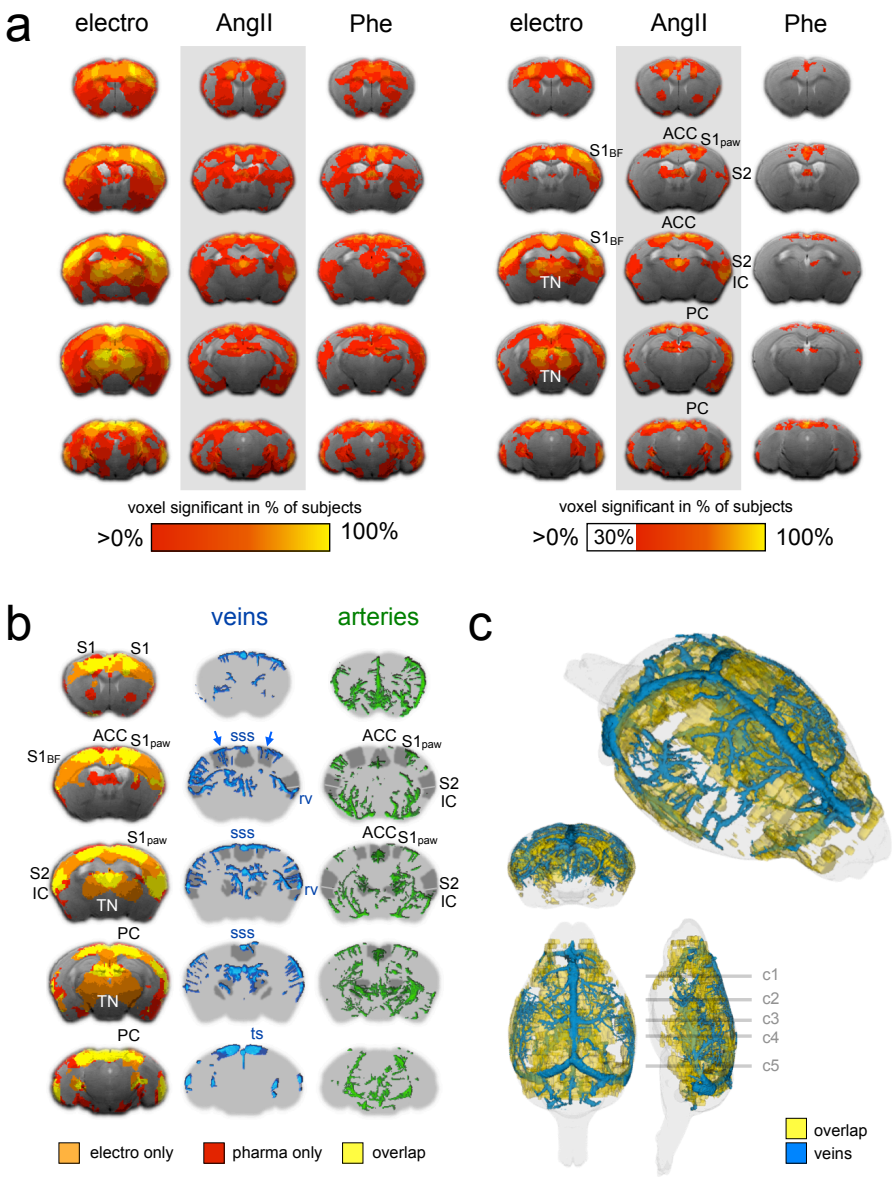

Fig. 8 – Conjunction analysis and co-localization with cerebral vasculature. a. Group conjunction of single subject statistic maps (cluster inference, default threshold of z=2.3, p<.05) for electrostimulation (n=9) and administration of AngII (n=6) and Phe (n=15). Single subjects were analyzed by GLM using the MABP as EV. **Left panel:** superimposed z-maps of all animals in the group. **Right panel:** same as in left panel but only voxels are displayed, which are significant in 30% of the animals. **b.** Difference map of significant voxels (group conjunction, 30% criterion) detected only for electrostimulation shown in orange, only for pharmacologically evoked blood pressure changes (AngII + Phe) in red and overlapping voxels from both conditions in yellow (**left column**). Superpositions with veins (**center column**) and arteries (**right column**) are displayed. Overlapping BOLD patterns co-localize with large veins in cortical regions of the neuromatrix: ACC with the superior saggital sinus (sss), S1 (particularly $S1_{paw}$) with penetrating branches of the sss (blue arrows), and S2 and IC with the rhinal vein (rv). PC aligns with the region between sss and the transverse sinuses (ts). Thalamic nuclei (TN) and lateral areas of the S1 including the barrel field ($S1_{BF}$) were only significant in response to electrostimulation. **c.** 3D rendering of BOLD clusters overlapping for electrostimulation and pharmacological tasks superimposed on the venous vessel tree. Note the activity patterns following the course of the venous vasculature.

ii) Neurovascular considerations

It is known that pial veins can induce strong BOLD effects within adjacent tissue. To verify whether the observed BOLD hot spots were associated with large vessels, a vascular brain atlas based on X-ray computed tomography (Dorr et al., 2007) was superimposed on the difference map (Fig. 8b, centre and right column). Comparing the venous vessel tree to BOLD patterns revealed an extensive overlap between the most significant regions and large superficial draining veins: the ACC with the superior saggital sinus from which a lateral branch runs just above the S1 and penetrates the paw region via large venules (Fig. 8b, centre column, blue arrows), and the IC and the S2 with the caudal rhinal vein. The PC resides at the position where the superior saggital sinus branches into the transverse sinuses. Further significant BOLD patterns align with the longitudinal hippocampal vein, superior olfactory sinus, and superficial temporal vein. The BOLD effects induced by systemic BP directly follow the course of large veins and venules in the murine brain (Fig. 8c). Notably, no large veins were found in the thalamic area where electrostimulation produced a BOLD signal but pharmacologically induced MABP increase did not.

iii) Exemplification

Elevations in MABP induced significant BOLD clusters that co-localized with cortical draining veins at a group level (Fig. 8b, c). This association was even more apparent in single subjects. Figure 9a shows the MABP in absolute values for an individual animal – rising from approximately 70-100 mmHg in response to angiotensin II. The BOLD response in the same animal is displayed below (Fig. 9b, ascertained by using a boxcar HRF as EV). To maintain spatial fidelity, the fMRI data were not registered to a reference space and were not smoothed. The statistical map was superimposed on susceptibility-weighted structural MRI data obtained for the same animal, showing large veins as dark lines (Fig. 9b, left column). Significant voxels were clearly aligned with large penetrating veins (Fig. 9b, centre column). When the statistical threshold was lowered, BOLD effects became distributed throughout in the entire mouse brain (Fig. 9b, right column), in most of the tested subjects.

The effect of transient MABP alterations on the BOLD signal was greatest at the superficial pial veins (Fig. 9c). The average signal of the anatomical hindpaw region of S1 exhibited BOLD signal magnitudes of 2.3% in the left and 1.8% in the right hemisphere. The voxel with the highest z-score (best voxel) within that region was located deeper in the cortex in the left hemisphere, and showed a maximum of 3.2%. The best voxel in the corresponding area of the right hemisphere, which was located in superficial layers, increased dramatically to 21.8%. For the ACC both best

voxels were similarly located within the central sinus, and reached maxima of 31.8% and 34.0% out of an average area magnitude of 2.4%.

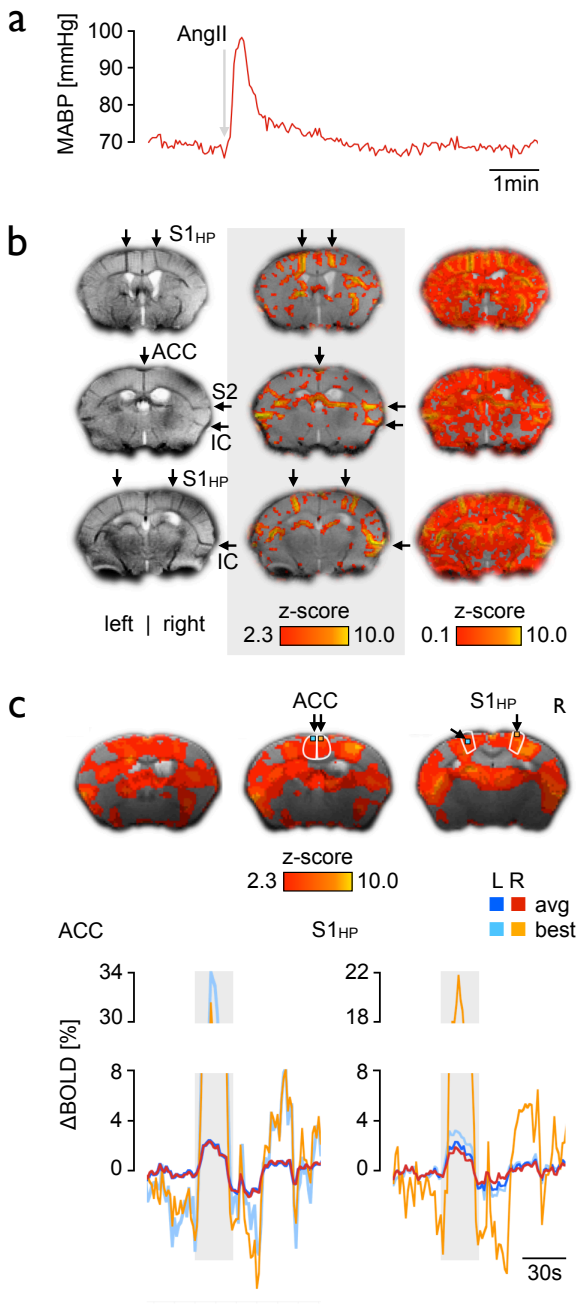

Fig. 9 – Exemplification. MABP time course and BOLD patterns for administration of AngII in a single subject. **a. MABP time course.** MABP magnitude reached approx. 30 mmHg in this subject. **b. Co-localization of BOLD responses with large draining veins. Left column:** Susceptibility weighted images of the same subject (neither smoothed nor registered to reference space). Note large draining veins cause dark contrasts in regions of the neuromatrix (indicated by black arrows) due to the large portion of deoxygenated blood. **Center column:** BOLD patterns induced by MABP changes follow the course of the dark veins (statistic threshold z=2.3). **Right column:** Statistic threshold reduced to z=0.1 reveals global BOLD patterns in the whole brain. **c. BOLD magnitudes in tissue and pial veins. Top panel:** Same animal as above, registered to a reference space and spatially smoothed. Significant voxels are blurred and cannot be assigned to penetrating veins. Contra- and ipsilateral ACC and $S1_{paw}$ are outlined in white, voxels with highest z-score in each area (best left /right) indicated by black arrows. **Bottom panel:** Average signal time courses plotted for ACC and $S1_{paw}$ and best voxels in response to AngII. These voxels reached BOLD signal magnitudes of up to 30% when located in superficial cortical layers. GLM analysis was performed by using MABP as EV in subfigure b and c.

To summarize i) in single subjects significant BOLD patterns were arranged in spatially distributed regions across the brain in a bilateral and symmetrical manner. ii) However, specific regions, ie. ACC, $S1_{paw}$, S2, IC, PC, were particularly susceptible to MABP alterations: iii) These regions accurately correspond to draining veins of the neurovasculature, and iv) showed BOLD signals whose magnitudes were significantly higher than those observed in the remaining brain tissue.

4. DISCUSSION

During the past years the central processing of somatosensation and pain has been increasingly studied using fMRI in mice. A network of cortical brain areas – the *neuromatrix*, often referred to as the "pain matrix" (Iannetti and Mouraux, 2010; Legrain et al., 2011) – has been described to reliably activate in response to noxious stimuli in mice (Baltes et al., 2011; Bosshard et al., 2010; Petrinovic et al., 2016; Schroeter et al., 2014) and humans (Duerden and Albanese, 2011; Tanasescu et al., 2016). However, there is growing evidence that the activity patterns observed in the murine "pain matrix" do not reflect underlying neural activity exclusively (Reimann et al., 2016; Schroeter et al., 2016; Schroeter et al., 2014). To address these issues, in this study we investigated the influence of the MABP on the BOLD signal in mice. We showed that electrostimulation of 1mA — a standard stimulus in somatosensory mouse fMRI (Baltes et al., 2011; Borsook and Becerra, 2011; Bosshard et al., 2010; Nasrallah et al., 2014; Petrinovic et al., 2016; Schroeter et al., 2014) — is sufficient to evoke substantial increases in MABP. We demonstrated that pharmacologically induced MABP increases of similar shape and magnitude as those observed in response to electrostimulation can also induce significant BOLD patterns, even in the absence of somatosensory stimuli. Those BOLD patterns were primarily located in cortical brain regions that form the *neuromatrix*, including the ACC and IC, S2 and $S1_{paw}$, as well as in the PC. Furthermore, these regions co-localized with large pial veins.

The close link between salient MABP changes and the *neuromatrix* has major implications for rodent BOLD fMRI studies in which those brain areas are the main focus of investigation (Baltes et al., 2011; Borsook and Becerra, 2011; Bosshard et al., 2010; Nasrallah et al., 2014; Petrinovic et al., 2016; Schroeter et al., 2014). BOLD patterns, which were reliably observed in structures of the "pain matrix", may not reflect specific nociceptive or somatosensory processing. Those regions are particularly prone to the translation of global increases in cerebral perfusion into significant BOLD effects. Nevertheless, we did observe BOLD effects in several regions which likely do reflect true neural activity. Those BOLD patterns were significant in animals receiving electrical stimulation, but not for pharmacologically induced MABP changes. These areas include regions in the ventral thalamic nuclei, which relay somatosensory input from the periphery to the cortex (Mo et al., 2017), and the lateral S1 including the barrel field, which takes part in unspecific processing of transient somatosensory input in mice, arousal and alertness (Bosman and Houweling, 2011; Mohajerani et al., 2011).

Stringent thresholding (primary cluster threshold of $p<0.001$; Woo et al., 2014; Eklund et al., 2016) improved the precision of detecting clusters in areas involved in somatosensory processing, for

example in the contralateral $S1_{paw}$. It also emphasized that thalamic nuclei showed higher z-scores for HRF than for MABP, which can be considered further evidence that those BOLD patterns were based on neurovascular coupling. Thresholding at $p<0.01$ revealed clusters in the ipsilateral $S1_{paw}$, which were not detected at $p<0.001$. Neural activity in the ipsilateral $S1_{paw}$ upon electrostimulation was reported for mice (Mohajerani et al., 2011) and rats (Uchida et al., 2017), thus correcting for the confounding effects of MABP using $p<0.001$ may increase the likelihood of type II error (false negatives). However, conservative thresholding fails to reliably correct for MABP evoked BOLD patterns, which can still heavily confound regions of interest in somatosensory studies like $S1_{paw}$.

In activated areas capillaries and upstream arterioles are dilated in response to neural activity (Hall et al., 2014; Hamilton, 2010). A global increase in cerebral perfusion pressure, induced by MABP elevations, further enhances local perfusion and consequently boosts BOLD effects, which originate from neurovascular coupling (Wang et al., 2006; Qiao et al., 2007; Jeffrey-Gauthier et al., 2013; Uchida et al., 2017).

In the present study, we induced transient increases in MABP with the endogenous hormone AngII and the synthetic α1-adrenergic receptor agonist Phe. Both agents act predominantly on smooth muscle cells of resistance vessels outside the brain, and do not cross the blood brain barrier under physiological conditions (Faraci and Heistad, 1990). Circulating Phe was shown to have no direct effect on CBF (Drummond, 2012; Ogoh et al., 2011; Rogers et al., 1988), and is therefore used to study the influence of systemic blood pressure elevations on CBF (McCulloch and Turner, 2009; Rozet et al., 2006; Wagner et al., 2011). Interactions of AngII with the cerebral vasculature could not be completely excluded (Saavedra and Nishimura, 1999). However, given the high degree of similarity in the effects of the two agents, it is unlikely that any potential direct actions of AngII on the cerebral vasculature or neurovascular units had any effect on the appearance of significant BOLD patterns. Therefore we interpret that for both agents the BOLD patterns were induced by an increased influx of oxygenated blood into the brain, driven by transient MABP elevations, which were caused by extracerebral vasoconstriction.

This conclusion is further supported by the symmetrical BOLD patterns revealed in the conjunction analysis, and the observation that BOLD effects were distributed throughout the entire brain when the statistical threshold was lowered. It is expected that brain regions with similar vascular density and vascular properties (i.e. local resistance, responsiveness to perfusion pressure) express acute global increases in CBF with comparable changing rates in blood oxygenation (Wang et al., 2006). Notably, changes in blood oxygenation occur only in the micro- and postcapillary vasculature, but not in the arterial vessel tree, in which oxygen saturation is already close to 100% (Kim and Ogawa,

2012). The symmetrical and bilateral BOLD patterns we observed upon both electrostimulation and pharmacologically induced MABP changes reflected the symmetry of the venous cerebrovascular architecture. The best correlation between the MABP and BOLD signal time course was found in large superficial veins. Those veins collect blood from large and small pial veins that cover the surface of the hemispheres and drain large parts of the cortex, which therefore leads to profound rises in blood oxygenation during increases in global perfusion of the brain. Additionally, voxels located entirely within those large veins reflect exclusively the T_2* of blood, and are not influenced by the T_2* of brain tissue (Kim and Ogawa, 2012). Analysis of raw, unsmoothed data revealed that highly significant voxels precisely followed the course of large branches of superficial veins, which penetrated the cortex into the areas of the "pain matrix". Lowering the statistical threshold revealed BOLD effects that emerged first in parts of the cortex and to a lesser extent in subcortical areas. This can be explained by differences in the blood volume fraction of voxels (Kim and Ogawa, 2012) indicating differences in vascular density in the respective areas (Gozzi et al., 2007).

Whereas heart rate decreased upon administration of the vasoconstrictors, it increased upon electrostimulation. The mechanisms behind these opposing responses are well established, as reviewed in Dampney (2016). Vasoconstrictors increase MABP, which in turn results in decreased heart rate via the baroreceptor reflex. However, physical stressors like electrostimulation trigger simultaneous increases in both MABP and heart rate by activating sympathetic neurons in spinal cord and brain stem. At least two structures of the "pain matrix", ACC and IC, are also known to be involved in the central control of systemic blood pressure (Oppenheimer and Cechetto, 2016). Although the involvement of these structures is not essential for basic cardiovascular reflex regulation (Dampney, 2016), a neurovascular contribution to the BOLD effects in those areas cannot be excluded. Nevertheless, this is not required to explain the observed BOLD patterns, since the dominating effects clearly derived from large penetrating pial veins. Spatial smoothing for statistical reasons (Woo et al., 2014; Worsley et al., 1996), and registration of the data to a common reference space substantially blurred the precise BOLD profiles of those veins, suffusing entire anatomical regions of the "pain matrix". Given that both spatial smoothing and registration are commonly used data processing steps in BOLD fMRI (Eklund et al., 2016; Stelzer, 2014), this could easily lead to the misinterpretation of macrovascular effects as strong BOLD effects in the microvasculature caused by area-specific neurovascular coupling (Turner, 2002).

The precise co-localization of large pial veins with the "pain matrix" constitutes a serious problem for the canonical analysis of fMRI data, since alterations in MABP correlated strongly and inherently with the stimuli, which evoked them. This is emphasized by the observation of almost

identical spatial BOLD distributions in the mouse brain, whether we applied the MABP or an HRF based on the electrostimulation paradigm as EV for all conditions (electrostimulation and pharmacological interventions). Recent findings have led to the view that the "pain matrix" is not pain specific, but rather it responds to a variety of sensory stimuli (e.g. flashing lights, surprising sounds, unexpected somatosensory input) as long as they are salient (Mouraux et al., 2011). The *neuromatrix* is essentially activated by the same stimuli that potentially provoke transient elevations in MABP. Given the fact that MABP-evoked BOLD effects occur predominantly in areas which are expected to reflect neural activity in response to salient stimuli, BOLD effects in the murine *neuromatrix* should be interpreted with caution. This also applies to murine connectivity studies in which the correlation of signal time courses across brain regions is a measure of functional connectivity (van den Heuvel and Pol, 2010). The discrete areas of the *neuromatrix* tend to oscillate with alterations in MABP due to their similar vascular properties; e.g. suggesting significantly increased network activity in the "pain matrix" of hypertensive animals.

Cerebral autoregulatory responses, which maintain CBF relatively constant in the face of systemic blood pressure changes, were reported to be largely preserved under low dose isoflurane in mechanically ventilated animals (Lee et al., 1994; Lee et al., 1995; Masamoto and Kanno, 2012). Yet our results confirm that abrupt increases in MABP are sufficient to confound BOLD fMRI measurements (Kalisch et al., 2001; Tuor et al., 2002; Tuor et al., 2007; Wang et al., 2006) even when the peak values in MABP did not exceed 100 mmHg. Therefore, an autoregulatory range of 60-120 mmHg, in which abrupt changes of MABP do not result in CBF alterations, as previously described (Ferrari et al., 2012; Gozzi et al., 2007), could not be confirmed by our results. While differences between species (mice vs. rats) cannot be excluded as an explanation, this finding can be also conclusively explained by the high transition rates in MABP, which we induced to mimic the MAPB response to electrical stimuli. However, the BOLD signal does not directly reflect CBF, but is also dependent on changes in blood volume and oxygen consumption (Kim and Ogawa, 2012). To draw accurate inferences on cerebral autoregulation would require direct recording of CBF – a comparable assessment in mice is still pending. Nevertheless, our results indicate that a range in which the BOLD signal (and likely also CBF) is unaffected by abrupt MABP alterations cannot be defined without considering magnitude and transition rate. The occurrence of abrupt MABP changes of up to 30 mmHg, which are observed in nociception and stress in humans (Carter et al., 2005; Peckerman et al., 1991), implies that the effects described in this work may also be of relevance for human fMRI studies.

It is well documented that dynamic autoregulation does not sufficiently buffer strong and abrupt elevations in systemic blood pressure, which leads to transient increases in CBF, even in healthy and conscious humans (Armstead, 2016; Tzeng and Ainslie, 2013). The onset of the fight-or-flight response (Cannon, 1932) is typically accompanied by strong and abrupt MABP elevations and demands a simultaneous engagement of multiple brain regions whose proper performance is vital during life-threatening situations. Since oxygen delivery can limit effectual brain function (Leithner and Royl, 2014), a cardiovascular support mechanism, based on abrupt MABP elevations, is conceivable to provide additional energy supply to brain areas, which execute initial processes to protect the organism from sudden and unexpected threats. The *neuromatrix* has been proposed to remap potentially harmful stimuli in reference to the body orientation in order to initiate prompt and appropriate motor responses (Haggard et al., 2013). Its activation is triggered by salient events (Mouraux et al., 2011), which are prone to provoke abrupt increases in MABP. Also the parietal cortex is involved in spatial awareness to potential threats, multimodal integration and planning of precise motor actions including goal directed head and limb movements (Cohen and Andersen, 2002; Stein and Stanford, 2008; Wilber et al., 2014). From an evolutionary perspective, a cardiovascular support mechanism that provides additional energy supply to activated brain regions especially required in the initial phase of fight and flight is an attractive hypothesis (Fig. 10), which has thus far not been proposed. The degree to which areas like the parietal cortex or those of the *neuromatrix* thereby benefit from their positions in proximity to large draining veins is not fully clarified, and remains an objective for future investigations.

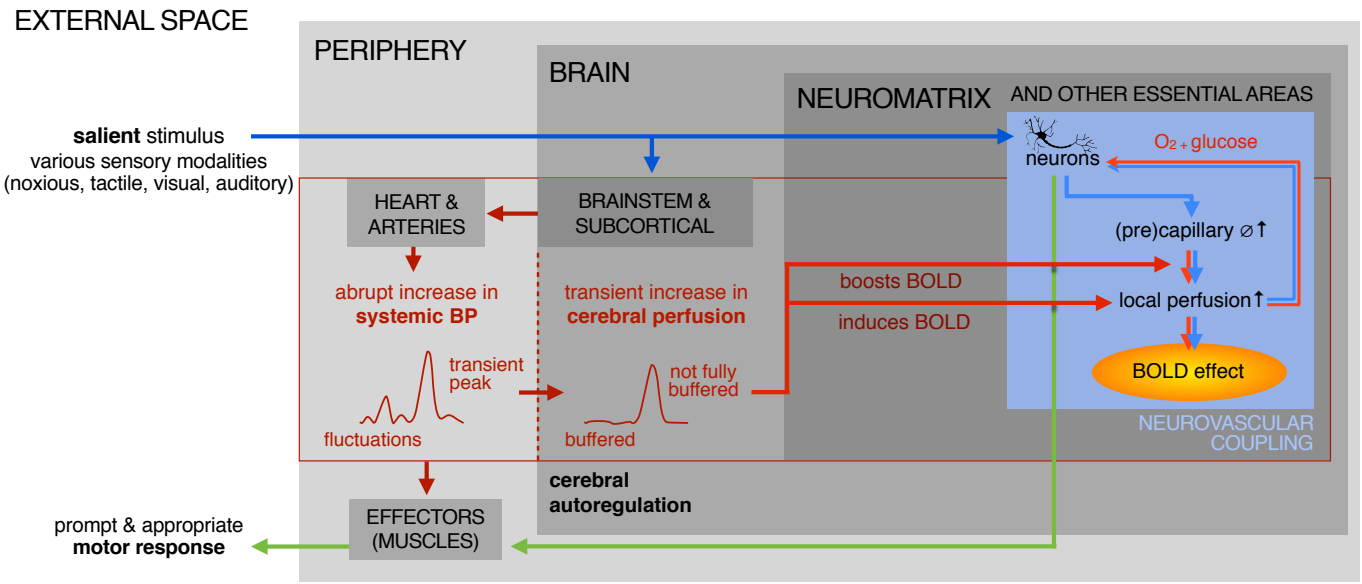

Fig. 10 – A cardiovascular support mechanism for central nervous energy supply in the initial phase of fight-or-flight situations. Salient sensory information is transmitted into the neuromatrix, which remaps perceived stimuli from the body space into the external space to initiate prompt and appropriate motor responses (dark blue and green arrow paths). Activity-mediated vasodilation causes increased local perfusion and thus local energy supply of the activated brain regions (neurovascular coupling, light blue arrows in light blue box). The BOLD effect occurs as a result of increased blood oxygenation in (post-) capillary vessels, serving as a surrogate for neural activity. Yet salient stimuli are also prone to evoke abrupt elevations in systemic blood pressure (BP), which are not sufficiently buffered by cerebral autoregulation, causing transient global increases in cerebral perfusion (dark red arrow paths). This can induce significant BOLD effects in large veins and regions of high vascular density, without any neurovascular contribution, while BOLD effects in activated areas get boosted due to neurovascular-induced vasodilation (light red arrow paths), which leads to additional oxygen /nutrient supply of activated neurons (light red arrows in light blue box). In the face of sudden, unexpected threats a cardiovascular mechanism that supports the energy supply of brain regions especially required in the initial phase of fight or flight is conceptually appealing to ensure proper motor actions and thus protect the organism from potential injury and death.

5. CONCLUSION

It has been proposed that somatosensory mouse fMRI may reveal BOLD effects of non-neural origin. In this study we provide the first direct evidence that electrostimulation of the murine paw at 1mA is sufficient to evoke substantial increases in MABP. By pharmacologically mimicking this effect, we demonstrated that MABP elevations of this magnitude can evoke consistent bilateral BOLD patterns, primarily in cortical regions including S1, S2, ACC and IC, likely caused by global hyperperfusion of the cerebrovasculature. Statistical inference cannot reliably account for controlling MABP induced BOLD signals, since they can develop temporal profiles very similar to the expected HRF, and can appear with high z-scores at the group level. Therefore, we conclude that BOLD signals, which have been observed in murine somatosensory fMRI in areas of the "pain matrix", are prone to be confounded by MABP and could potentially reflect the increase of MABP, rather than somatosensory processing. BOLD effects in the somatosensory relay nuclei of the ventral thalamus and the barrel fields of S1 were evoked in response to electrostimulation, but not by pharmacologically induced MABP elevations, and thus likely reflect neural activity. MABP-induced increase in perfusion of activated areas might be further enhanced by neural-induced vasodilation. However, the confounding effects of MABP changes in areas of the murine *neuromatrix* call into question conclusions about these regions drawn from somatosensory fMRI studies in rodents in which the MABP was challenged. Confining abrupt MABP alterations within a range of 60-120 mmHg does not exclude potential confounding effects on BOLD fMRI data. Future BOLD fMRI studies will require that MABP be taken into consideration, either by establishing protocols to sufficiently suppress systemic blood pressure changes, or by developing more sophisticated techniques to distinguish BOLD signals that arise in response to neural activity from those that might be triggered by systemic blood pressure alone.

Most of the MABP-sensitive regions found in this study belong to the *neuromatrix* and parietal cortex, which are crucial for immediate reactions to potential threats. We hypothesize the existence of a vascular support mechanism, which utilizes transient systemic blood pressure changes to provide sufficient energy supply to the *neuromatrix* and other essential areas involved in the initial phase of fight-or-flight situations. The critical role that this mechanism could play in the survival of an animal is conceptually appealing from an evolutionary perspective, and should be pursued in further investigations.

6. Literature

Armstead, W.M., 2016. Cerebral Blood Flow Autoregulation and Dysautoregulation. Anesthesiol. Clin. 34, 465-477.

Avants, B.B., Tustison, N.J., Song, G., Cook, P.A., Klein, A., Gee, J.C., 2011. A reproducible evaluation of ANTs similarity metric performance in brain image registration. Neuroimage 54, 2033-2044.

Baltes, C., Bosshard, S., Mueggler, T., Ratering, D., Rudin, M., 2011. Increased blood oxygen level-dependent (BOLD) sensitivity in the mouse somatosensory cortex during electrical forepaw stimulation using a cryogenic radiofrequency probe. NMR Biomed. 24, 439-446.

Borsook, D., Becerra, L., 2011. CNS animal fMRI in pain and analgesia. Neurosci. Biobehav. Rev. 35, 1125-1143.

Bosman, L., Houweling, A.R., 2011. Anatomical pathways involved in generating and sensing rhythmic whisker movements. Front. Integr. Neurosci. 5, 1-28.

Bosshard, S.C., Baltes, C., Wyss, M.T., Mueggler, T., Weber, B., Rudin, M., 2010. Assessment of brain responses to innocuous and noxious electrical forepaw stimulation in mice using BOLD fMRI. Pain 151, 655-663.

Cannon, W.B., 1932. The Wisdom of the Body. Norton.

Carter, J.R., Kupiers, N.T., Ray, C.A., 2005. Neurovascular responses to mental stress. J. Physiol. 564, 321-327.

Cohen, Y.E., Andersen, R.A., 2002. A common reference frame for movement plans in the posterior parietal cortex. Nat. Rev. Neurosci. 3, 553-562.

Dampney, R.A.L., 2016. Central neural control of the cardiovascular system: current perspectives. Adv. Physiol. Educ. 40, 283–296.

Dorr, A., Sled, J.G., Kabani, N., 2007. Three-dimensional cerebral vasculature of the CBA mouse brain: A magnetic resonance imaging and micro computed tomography study. Neuroimage 35, 1409-1423.

Drummond, J.C., 2012. Cerebral blood flow and the alpha-1 agonist bogeyman. Anesth. Analg. 114, 478-479.

Duerden, E.G., Albanese, M.-C., 2011. Localization of pain-related brain activation: A meta-analysis of neuroimaging data. Hum. Brain. Mapp. 34, 109-149.

Eklund, A., Nichols, T.E., Knutsson, H., 2016. Cluster failure: Why fMRI inferences for spatial extent have inflated false-positive rates. PMCID 28, 7900-7905.

Faraci, F.M., Heistad, D.D., 1990. Regulation of large cerebral arteries and cerebral microvascular pressure. Circ. Res. 66, 8-17.

Ferrari, L., Turrini, G., Crestan, V., Bertani, S., Cristofori, P., Bifone, A., Gozzi, A., 2012. A robust experimental protocol for pharmacological fMRI in rats and mice. J. Neurosci. Methods 204, 9-18.

Flaten, M.A., al'Absi, M., 2015. Neuroscience of Pain, Stress, and Emotion. Academic Press.

Friston, K.J., Fletcher, P., Josephs, O., Holmes, A., Rugg, M.D., & Turner, R., 1998. Event-related fMRI: Characterizing differential responses. Neuroimage, 7, 30–40.

Glover, G.H., 1999. Deconvolution of impulse response in event-related BOLD fMRI. Neuroimage 9, 416-29.

Gould, I.G., Tsai, P., Kleinfeld, D., Linninger, A., 2017. The capillary bed offers the largest hemodynamic resistance to the cortical blood supply. J Cereb Blood Flow Metab. 37, 52-68.

Gozzi, A., Ceolin, L., Schwarz, A., Reese, T., Bertani, S., Crestan, V., Bifone, A., 2007. A multimodality investigation of cerebral hemodynamics and autoregulation in pharmacological MRI. Magn. Reson. Imaging 25, 826-833.

Haggard, P., Iannetti, G.D., Longo, M.R., 2013. Spatial sensory organization and body representation in pain perception. Curr. Biol. 23, R164-176.

Hall, C.N., Reynell, C., Gesslein, B., Hamilton, N.B., Mishra, A., Sutherland, B.A., O'Farrell, F.M., Buchan, A.M., Lauritzen, M., Attwell, D., 2014. Capillary pericytes regulate cerebral blood flow in health and disease. Nature 508, 55-60.

Hamilton, N.B., 2010. Pericyte-mediated regulation of capillary diameter: a component of neurovascular coupling in health and disease. Front. Neuroenergetics 2, 1-5.

Iannetti, G.D., Mouraux, A., 2010. From the neuromatrix to the pain matrix (and back). Exp. Brain Res. 205, 1-12.

Janke AL, U.J., Kurniawan N, Paxinos G, Keller M, Yang Z, Richards K, Egan G, Petrou S,Galloway G, Reutens D., 2012. 15µm average mouse models in Waxholm space from 16.4T 30µm images. In 20th Annual ISMRM Scientific Meeting and Exhibition, Melbourne, Australia.

Jeffrey-Gauthier, R., Guillemot, J.P., Piche, M., 2013. Neurovascular coupling during nociceptive processing in the primary somatosensory cortex of the rat. Pain 154, 1434-1441.

Jenkinson, M., Beckmann, C.F., Behrens, T.E.J., Woolrich, M.W., Smith, S.M., 2012. FSL. Neuroimage 62, 782-790.

Kalisch, R., Elbel, G.K., Gossl, C., Czisch, M., Auer, D.P., 2001. Blood pressure changes induced by arterial blood withdrawal influence bold signal in anesthesized rats at 7 Tesla: implications for pharmacologic mri. Neuroimage 14, 891-898.

Kim, S.G., Ogawa, S., 2012. Biophysical and physiological origins of blood oxygenation level-dependent fMRI signals. J. Cereb. Blood Flow Metab. 32, 1188-1206.

Lee, J.G., Hudetz, A.G., Smith, J.J., Hillard, C.J., Bosnjak, Z.J., Kampine, J.P., 1994. The effects of halothane and isoflurane on cerebrocortical microcirculation and autoregulation as assessed by laser-Doppler flowmetry. Anesth. Analg. 79, 58-65.

Lee, J.G., Smith, J.J., Hudetz, A.G., Hillard, C.J., 1995. Laser-Doppler measurement of the effects of halothane and isoflurane on the cerebrovascular CO2 response in the rat. Anesth. Analg. 80, 696-702.

Legrain, V., Iannetti, G.D., Plaghki, L., Mouraux, A., 2011. The pain matrix reloaded: a salience detection system for the body. Prog. Neurobiol. 93, 111-124.

Leithner, C., Royl, G., 2014. The oxygen paradox of neurovascular coupling. J. Cereb. Blood Flow Metab. 34, 19-29.

Mancini, F., Bauleo, A., Cole, J., Lui, F., Porro, C.A., Haggard, P., Iannetti, G.D., 2014. Whole-body mapping of spatial acuity for pain and touch. Ann. Neurol. 75, 917-924.

Manjon, J.V., Coupe, P., Marti-Bonmati, L., Collins, D.L., Robles, M., 2010. Adaptive non-local means denoising of MR images with spatially varying noise levels. J. Magn. Reson. Imaging 31, 192-203.

Masamoto, K., Kanno, I., 2012. Anesthesia and the quantitative evaluation of neurovascular coupling. J. Cereb. Blood Flow Metab. 32, 1233-1247.

McCulloch, T.J., Turner, M.J., 2009. The Effects of Hypocapnia and the Cerebral Autoregulatory Response on Cerebrovascular Resistance and Apparent Zero Flow Pressure During Isoflurane Anesthesia. Anesth. Analg. 108, 1284-1290.

Melzack, R., 1989. Labat lecture. Phantom limbs. Reg. Anesth. 14, 208-211.

Mo, C., Petrof, I., Viaene, A.N., Sherman, S.M., 2017. Synaptic properties of the lemniscal and paralemniscal pathways to the mouse somatosensory thalamus. Proc. Natl. Acad. Sci. USA 114, 6212-6221.

Mohajerani, M.H., Aminoltejari, K., Murphy, T.H., 2011. Targeted mini-strokes produce changes in interhemispheric sensory signal processing that are indicative of disinhibition within minutes. Proc. Natl. Acad. Sci. USA 108, 8932-8933.

Morton, D., Jones, A., Sandhu, J., 2016. Brain imaging of pain: state of the art. J. Pain Res. 9, 613-624.

Mouraux, A., Diukova, A., Lee, M.C., Wise, R.G., Iannetti, G.D., 2011. A multisensory investigation of the functional significance of the "pain matrix". Neuroimage 54, 2237-2249.

Nasrallah, F.A., Tay, H.-C., Chuang, K.-H., 2014. Detection of functional connectivity in the resting mouse brain. Neuroimage 86, 417-424.

Niendorf, T., Pohlmann, A., Reimann, H.M., Waiczies, H., Peper, E., Huelnhagen, T., Seeliger, E., Schreiber, A., Kettritz, R., Strobel, K., Ku, M.-C., Waiczies, S., 2015. Advancing Cardiovascular, Neurovascular, and Renal Magnetic Resonance Imaging in Small Rodents Using Cryogenic Radiofrequency Coil Technology. Front. Pharmacol. 6, 704.

Ogawa, S., Lee, T.M., Kay, A.R., Tank, D.W., 1990. Brain Magnetic Resonance Imaging with Contrast Dependent on Blood Oxygenation. Proc. Natl. Acad. Sci. USA 87, 9868-9872.

Ogoh, S., Sato, K., Fisher, J.P., Seifert, T., Overgaard, M., Secher, N.H., 2011. The effect of phenylephrine on arterial and venous cerebral blood flow in healthy subjects. Clin. Physiol. Funct. Imaging 31, 445-451.

Oppenheimer, S., Cechetto, D., 2016. The insular cortex and the regulation of cardiac function. Compr. Physiol. 6, 1081-1133.

Peckerman, A., Saab, P.G., McCabe, P.M., 1991. Blood pressure reactivity and perception of pain during the forehead cold pressor test. Psychophysiology 28, 485-495.

Petrinovic, M.M., Hankov, G., Schroeter, A., Bruns, A., Rudin, M., von Kienlin, M., Künnecke, B., Mueggler, T., 2016. A novel anesthesia regime enables neurofunctional studies and imaging genetics across mouse strains. Sci. Rep. 6, 1-12.

Paulson, O.B., 2002. Blood-brain barrier, brain metabolism and cerebral blood flow. Eur. Neuropsychopharmacol. 6, 495-501.

Poline, J.-B., Brett, M., 2012. The general linear model and fMRI: Does love last forever? Neuroimage 62, 871-880.

Qiao, M., Rushforth, D., Wang, R., Shaw, R.A., Tomanek, B., Dunn, J.F., Tuor, U.I., 2007. Blood-oxygen-level-dependent magnetic resonance signal and cerebral oxygenation responses to brain

activation are enhanced by concurrent transient hypertension. J. Cereb. Blood Flow Metab. 27, 1280–1289.

Reimann, H.M., Hentschel, J., Marek, J., Huelnhagen, T., Todiras, M., Kox, S., Waiczies, S., Hodge, R., Bader, M., Pohlmann, A., Niendorf, T., 2016. Normothermic Mouse Functional MRI of Acute Focal Thermostimulation for Probing Nociception. Sci. Rep. 6, 1-17.

Rogers, A.T., Stump, D.A., Gravlee, G.P., Prough, D.S., Angert, K.C., Wallenhaupt, S.L., Roy, R.C., Phipps, J., 1988. Response of cerebral blood flow to phenylephrine infusion during hypothermic cardiopulmonary bypass: influence of PaCO2 management. Anesthesiology 69, 547-551.

Rozet, I., Vavilala, M.S., Lindley, A.M., Visco, E., Treggiari, M., Lam, A.M., 2006. Cerebral Autoregulation and CO2 Reactivity in Anterior and Posterior Cerebral Circulation During Sevoflurane Anesthesia. Anesth. Analg. 102, 560-564.

Saavedra, J.M., Nishimura, Y., 1999. Angiotensin and cerebral blood flow. Cell. Mol. Neurobiol. 5, 553–573.

Schroeter, A., Grandjean, J., Schlegel, F., Saab, B.J., Rudin, M., 2016. Contributions of structural connectivity and cerebrovascular parameters to functional magnetic resonance imaging signals in mice at rest and during sensory paw stimulation. J. Cereb. Blood Flow Metab. 37, 2368-2382.

Schroeter, A., Schlegel, F., Seuwen, A., Grandjean, J., Rudin, M., 2014. Specificity of stimulus-evoked fMRI responses in the mouse: the influence of systemic physiological changes associated with innocuous stimulation under four different anesthetics. Neuroimage 94, 372-384.

Stein, B.E., Stanford, T.R., 2008. Multisensory integration: current issues from the perspective of the single neuron. Nat. Rev. Neurosci. 9, 255-266.

Stelzer, J., 2014. Deficient approaches to human neuroimaging. Front. Hum. Neurosci. 8, 1-16.

Tanasescu, R., Cottam, W.J., Condon, L., Tench, C.R., Auer, D.P., 2016. Functional reorganisation in chronic pain and neural correlates of pain sensitisation: A coordinate based meta-analysis of 266 cutaneous pain fMRI studies. Neurosci. Biobehav. 68, 120-133.

Tuor, U.I., McKenzie, E., Tomanek, B., 2002. Functional magnetic resonance imaging of tonic pain and vasopressor effects in rats. Magn. Reson. Imaging 20, 707-712.

Tuor, U.I., Wang, R., Zhao, Z., Foniok, T., Rushforth, D., Wamsteeker, J.I., Qiao, M., 2007. Transient Hypertension Concurrent with Forepaw Stimulation Enhances Functional MRI Responsiveness in Infarct and Peri-Infarct Regions. J. Cereb. Blood Flow Metab. 27, 1819-1829.

Turner, R., 2002. How Much Cortex Can a Vein Drain? Downstream Dilution of Activation-Related Cerebral Blood Oxygenation Changes. Neuroimage 16, 1062-1067.

Tustison, N.J., Avants, B.B., 2013. Explicit B-spline regularization in diffeomorphic image registration. Front. Neuroinform. 7, 39.

Tzeng, Y.-C., Ainslie, P.N., 2013. Blood pressure regulation IX: cerebral autoregulation under blood pressure challenges. Eur. J. Appl. Physiol. 114, 545-559.

Uchida, S., Bois, S., Guillemot, J.-P., Leblond, H., Piché, M., 2017. Systemic blood pressure alters cortical blood flow and neurovascular coupling during nociceptive processing in the primary somatosensory cortex of the rat. Neuroscience 343, 250-259.

Ullmann, J.F.P., Watson, C., Janke, A.L., Kurniawan, N.D., Reutens, D.C., 2013. A segmentation protocol and MRI atlas of the C57BL/6J mouse neocortex. Neuroimage, 1-8.

van den Heuvel, M.P., Pol, H.E.H., 2010. Exploring the brain network: A review on resting-state fMRI functional connectivity. Eur. Neuropsychopharmacol. 20, 519-534.

Wagner, B.P., Ammann, R.A., Bachmann, D., Born, S., 2011. Rapid assessment of cerebral autoregulation by near-infrared spectroscopy and a single dose of phenylephrine. Pediatr. Res. 69, 436–441.

Wang, R., Foniok, T., Wamsteeker, J.I., Qiao, M., Tomanek, B., Vivanco, R.A., Tuor, U.I., 2006. Transient blood pressure changes affect the functional magnetic resonance imaging detection of cerebral activation. Neuroimage 31, 1-11.

Watson, C., Janke, A.L., Hamalainen, C., Bagheri, S.M., Paxinos, G., Reutens, D.C., Ullmann, J.F.P., 2017. An ontologically consistent MRI-based atlas of the mouse diencephalon. Neuroimage, 1-26.

Wilber, A.A., Clark, B.J., Demecha, A.J., Mesina, L., Vos, J.M., McNaughton, B.L., 2014. Cortical connectivity maps reveal anatomically distinct areas in the parietal cortex of the rat. Front. Neural Circuits 8, 1-15

Woo, C.W., Krishnan, A., Wager, T.D., 2014. Cluster-extent based thresholding in fMRI analyses: pitfalls and recommendations. Neuroimage 91, 412-419.

Worsley, K.J., Marrett, S., Neelin, P., Vandal, A.C., 1996. A unified statistical approach for determining significant signals in images of cerebral activation. Hum. Brain. Mapp. 4, 58-73.

ACKNOWLEDGEMENTS

We wish to acknowledge David Reutens and Jeremy Ullmann (Centre for Advanced Imaging, University of Queensland, Brisbane, Australia) for their support and for the early provision of atlas delineation data of the murine diencephalon, and Kamil Ugurbil (Center for Magnetic Resonance Research, Department of Radiology, University of Minnesota, Minneapolis, USA) for discussions and advice.